Proceedings of the Jangjeon Mathematical Society
27 (2024), No. 3, pp. 485 – 510

www.jangjeon.or.kr
http://dx.doi.org/10.17777/pjms2024.27.3.485

WAVELET ANALYSIS OF VISCOELASTIC MAXWELL FLUID FOR CATTANEO - CHRISTOV HEAT FLUX MODEL

LAKSHMI B. N., SUMANA KRISHNA PRASAD, ASHA C. S.,
ACHALA L. NARGUND, LAXMI RATHOUR*, AND LAKSHMI NARAYAN MISHRA

Abstract. The study has been carried out on the boundary layer flow and heat transfer analysis in an MHD viscoelastic Maxwell fluid using the Cattaneo - Christov heat flux model. The effect of MHD on the Maxwell fluid over a stretching surface is investigated in the presence of suction/injection parameter. The nonlinear system of governing equations along with the boundary conditions is reduced into a set of coupled ordinary differential equations using a suitable similarity transformation. The nonlinearity of the equations is dealt with quasilinearization technique. The numerical solutions of resultant equations are determined using the Chebyshev wavelet collocation method and the Haar wavelet collocation method with the help of MATLAB software. The obtained results are compared and represented in terms of graphs and tables. The effect of various physical parameters such as elasticity parameter (Deborah number), heat flux relaxation time parameter, magnetic parameter (Hartmann number), viscous dissipation (Eckert number), Prandtl number and suction/injection parameter on velocity and temperature profiles are well discussed. The numerical values of skin friction coefficient $f''(0)$ and wall temperature gradient $\theta'(0)$ are also tabulated and compared to existing literature in limiting case. Error analysis has been carried out to check the convergence of the numerical scheme.

2000 Mathematics Subject Classification. 76A10, 65T60.

Keywords and phrases. Maxwell fluid, Cattaneo - Christov heat flux model, Chebyshev wavelets, Haar wavelets, quasilinearization, stretching surface, MHD, suction/injection, error analysis.

1. Nomenclature

x, y	tangential and normal distances
u, v	velocity components in the x and y axis
η, ψ	similarity variables
f, θ	dimensionless stream and temperature functions
$'$	derivative with respect to η
σ	electrical conductivity of the fluid
B_0	applied uniform magnetic field
λ_1	fluid relaxation time
λ_2	thermal relaxation time
α	thermal diffusivity
T	temperature of fluid
T_w	temperature at the wall

*Corresponding author.

T_∞	ambient fluid temperature
k	thermal conductivity
c_p	specific heat at constant pressure
v_0	suction/injection velocity
ρ	fluid density
a	stretching rate/positive constant
μ	dynamic viscosity
ν	kinematic viscosity
β	elasticity parameter (Deborah number)
γ	non-dimensional thermal relaxation time parameter
Pr	Prandtl number
Ec	Eckert number
S	suction/injection parameter
Mn	magnetic parameter (Hartmann number)
τ_w	surface shear stress
Re_x	local Reynolds number
Nu_x	local Nusselt number

2. Introduction

In recent years, a lot of investigation has been done on Maxwell fluid. It is the most widely used and the simplest model of viscoelastic fluid. The upper convected Maxwell (UCM) fluid gained a remarkable attention in the past few years. An elastic term relative to the Newtonian fluid model is present in UCM fluid which shows the influence of elastic force on the flow and heat transfer of the viscoelastic fluid [1]. The UCM fluid has the constitutive equation of the form,

$$\tau + \lambda\Big[\frac{D}{Dt} - \nabla u.\tau - \tau.\nabla u^T\Big] = \mu(\nabla u + \nabla u^T), \tag{1}$$

where $\frac{D}{Dt}$ is the material time derivative, which gives the relation between the stress tensor τ and the velocity gradient ∇u [2]. In this line of investigation, Sadeghy et al. [3] have done the theoretical analysis of the flow of UCM fluid in a quiescent fluid. They have employed perturbation method, fourth-order Runge-Kutta method and finite difference method to obtain the numerical solutions. They observed that as the value of Deborah number increases, the wall friction coefficient decreases for the flow. Abbas et al. [4] have considered the study of MHD upper convected Maxwell fluid in a channel in the presence of porous medium and obtained an analytical solution using homotopy analysis method (HAM).

Hayat et al. [5–7] have obtained the solution of MHD boundary layer flow of UCM fluid over a porous stretching sheet using HAM, including the effect of chemical reaction species past a porous shrinking sheet and stagnation point flow respectively. Hayat and Abbas [8] analyzed the two-dimensional boundary layer flow of UCM fluid in a channel with chemical reaction using HAM. The work of Hayat et al. [9–11] also includes the investigation using HAM to obtain the solution of Maxwell fluid over a stretching surface in the presence of Soret & Dufour effects, radiation effects in the porous channel, over a moving surface with convective boundary conditions respectively. Tripathi et al. [12] presented a fractional Maxwell model for the peristaltic flow of viscoelastic fluid. The analytical approximate solutions were obtained by the homotopy perturbation method and compared with the solutions of the Adomian decomposition method.

Chaudhary et al. [13] have analyzed the effect of thermo-physical properties on convective heat transfer of magnetohydrodynamics slip flow due to a permeable moving plate using the shooting method. They noticed that the variable thermal conductivity enhances the velocity. Chaudhary et al. [14] have investigated the boundary layer flow of a nanofluid in a saturated porous medium over a moving plate with viscous dissipation using fourth order Runge-Kutta shooting technique. Their study reveals that the velocity and concentration profile increases while the temperature profile decreases with increasing porous medium parameters. Marasi et al. [15] used Adomian polynomials to take care of the nonlinear terms and solved linear and nonlinear partial differential equations by the differential transform method. Negero et al. [16] and Woldaregay et al. [17] applied the fitted mesh finite difference method to solve boundary value problems that are frequently encountered in the spatial diffusion of reactants and in control systems.

Abel et al. [18] have studied the effect of a magnetic field on the viscoelastic liquid flow and heat transfer over a stretching sheet with a nonuniform heat source. The study of an unsteady stretching surface embedded in a porous medium in the presence of suction/injection is considered by Mukhopadhyay in [19] and the effect of thermal radiation in Mukhopadhyay et al. [20]. Nadeem et al. [21] have analyzed the effect of MHD, elasticity and nanoparticles on the boundary layer flow and the heat transfer of Maxwell fluid past a stretching sheet graphically. Siri et al. [22] investigated the boundary layer flow of viscoelastic fluid over a stretching surface in the presence of suction/injection parameters. Heat transfer of the fluid is analyzed using the Cattaneo - Christov heat flux model. The effect of various physical parameters on velocity and temperature profiles is discussed. Numerical solutions obtained by the Haar wavelet quasilinearization method and the RK Gill method are compared. They observed that the suction/injection parameter decreases the skin friction coefficient. Wahid et al. [23] have considered and examined the magnetohydrodynamics slip Darcy flow of viscoelastic fluid over a stretching surface in a porous medium with the presence of thermal radiation and viscous dissipation.

Sankar et al. [24, 25] have investigated the effects of the location of a discrete heating and salting segment on double-diffusive natural convection in a vertical porous annulus numerically using the implicit finite difference technique. They observed that the average Sherwood number increases with the Lewis number, while for the average Nusselt number the effect is opposite, also their results showed that when the size of the heater is smaller, the heat transfer rates are higher. Girish et al. [26] have obtained the numerical solution of the flow problem due to double-passage annuli filled with fluid-saturated porous media using the implicit finite difference method. They noticed that the temperature profile enhances with channel height and shifting baffle towards the inner wall but it reduces with an increase in the values of Grashof number and Darcy number towards an adiabatic wall. Reddy et al. [27] have considered the computational study of buoyant convection and heat dissipation processes of hybrid nanoliquid saturated in an inclined porous annulus. They have used the time-splitting Alternating Direction Implicit and line over-relaxation methods to obtain the numerical simulations. Their results revealed that when a stronger magnetic field is applied, it retards the flow movement as well as the heat dissipation rate due to its resistive effect.

Fourier [28] is the first person who proposed Fourier's law of heat conduction. Whenever there is a temperature difference between the objects or between the different parts of the same object, then there will be a concept of heat transfer. In 1822, in his book, he stated that "Heat flux is directly proportional to the magnitude of the temperature gradient" which is the description of the parabolic equation. However, this was the obstacle faced initially, since there were no objects satisfying these conditions. Later to avoid this, Cattaneo brought changes in Fourier's law by adding a relaxation time term. Then Christov [29] extended this law by replacing ordinary derivatives with Oldroyd's upper convected derivative. This is known as the Cattaneo - Christov heat flux model after Fourier's law of heat conduction. It is a generalization of Fourier's law. Fluid velocity is considered in the constitutive relationship between the heat flux and fluid temperature which shows that heat flux is related to fluid velocity as well as temperature gradient.

Tibullo et al. [30, 31] obtained the uniqueness and the structural solution for the temperature governing equation for the incompressible fluid by using the Cattaneo - Christov heat flux model. Straughan et al. [32] investigated thermal convection with the help of the Cattaneo - Christov heat flux model in the horizontal layer of an incompressible Newtonian fluid. Han et al. [33] have studied the boundary layer flow and heat transfer of a viscoelastic fluid by employing the upper convected Maxwell fluid model and the Cattaneo - Christov heat flux model over a stretching plate with a velocity slip boundary. The approximate analytical solutions are obtained by the homotopy analysis method. The impact of elasticity number, Prandtl number, slip coefficient and relaxation time of heat flux on velocity and temperature fields are analyzed and discussed. Mustafa [34] examined the rotating flow of viscoelastic fluid over a stretching surface by employing the Cattaneo - Christov heat flux model. Further, a lot of work on the Cattaneo - Christov heat flux model can be seen in [35–40].

At the beginning of the 1990s, wavelets were used to obtain the solution of differential equations. These wavelets have gained the remarkable attention of researchers. There are different types of wavelet families that can be applied. Based on this, we have to integrate wavelet functions to obtain the wavelet coefficients either by the Galerkin method or the collocation method [41]. Debnath and Shah [42] described a brief historical introduction to wavelet and wavelet transforms with their basic properties. Their study includes the discussion of types of wavelets with their graphical representation and applications. Adibi et al. [43] used Chebyshev wavelets to obtain the numerical solution of Fredholm integral equations of the first-kind. Hosseini et al. [44] obtained numerical solutions of ordinary differential equations using Chebyshev wavelet collocation method. They tested the spectral method for the same work which does not work well for ordinary differential equations. They also applied the Chebyshev wavelet Galerkin method for these kinds of problems.

Celik [45, 46] used Chebyshev wavelets to determine the solution of the Bessel differential equation of order zero, the Lane-Emden equation, a class of linear and nonlinear nonlocal boundary value problems of second and fourth order. They noted that the accuracy of the method increases as the number of grid points increases. Heydari et al. [47] obtained the solution of partial differential equations using the Chebyshev wavelet collocation method with less number of grid points which gave accurate solutions. Saeed [48] solved nonlinear boundary value problems using the wavelet Galerkin method with the quasilinearization technique by considering Daubechies scaling functions as Galerkin basis. Youssri et al. [49] have discussed the algorithm based on spectral second-kind Chebyshev wavelets in solving linear, nonlinear, singular and Bratu-type equations. They have noticed the efficiency and the accuracy of the method for less number of collocation points.

Sumana et al. [50–52] used the Haar wavelet collocation method to obtain the numerical solution of one-dimensional Fredholm integral equations of second-kind, non-homogeneous Burgers' equation with linear and periodic initial conditions and non-planar Burgers' equation. Sumana et al. [53] investigated the solution of time delayed Burgers' equations using Haar wavelets. The work of Sumana et al. [54] includes the study of Laplace and Poisson equations using two-dimensional 3-scale Haar wavelets. They have carried out the error analysis and shown that the solution improves as the level of wavelet resolution increases. Usman et al. [55] obtained the solution of MHD 3-D fluid flow in the presence of slip and thermal radiation effects using Chebyshev wavelets. They noticed that a suitable selection of stretching ratio parameter will help in hastening the heat transfer rate for a fixed value of of velocity slip parameter and in reducing the viscous drag over the stretching sheet. Also efficiency of the method was shown by convergent analysis.

Awashie et al. [56] have implemented the Chebyshev wavelet collocation method with an operational matrix of integration in the study of oil-water two-phase fluid flow in a reservoir. Wavelets have many applications in signal and image processing like compression, de-noising, discontinuity detection, audio enhancement and effects, edge detection, image fusion, image enhancement and many other applications. Sajid et al. [57] used the Legendre wavelet spectral collocation method to analyze the effect of radiation and slip on viscoelastic Walter's B fluid. Oruc et al. [58] considered the one-dimensional time-dependent coupled Burgers' equation along with the suitable initial and boundary conditions. The numerical solutions of this equation are obtained by using the Chebyshev wavelet collocation method. It is found that the proposed method gives accurate results in short cpu times. It is also examined that the method is computationally cheap and quite good for an even less number of collocation points. Recently, Jakhar et al. [59, 60] have used Wavelet–Fractal Transformation in Gradient Domain for image resolution enhancement.

The main aim of this paper is to study the momentum and heat transfer using the Cattaneo - Chistov heat flux model of an upper convected Maxwell fluid. The effect of physical parameters such as magnetic parameter, elasticity parameter, thermal relaxation time, Eckert number and Prandtl number are represented graphically and discussed. The current study is organized in the following way: In section 3 we describe the mathematical formulation of the problem under discussion and derive its governing equations along with appropriate boundary conditions. The method of solution is discussed in section 4 and the error analysis has been carried out in section 5. Numerical results and discussion are included in the section. 6. Finally, section 7 reveals the important findings that are summarized.

3. Mathematical Formulation

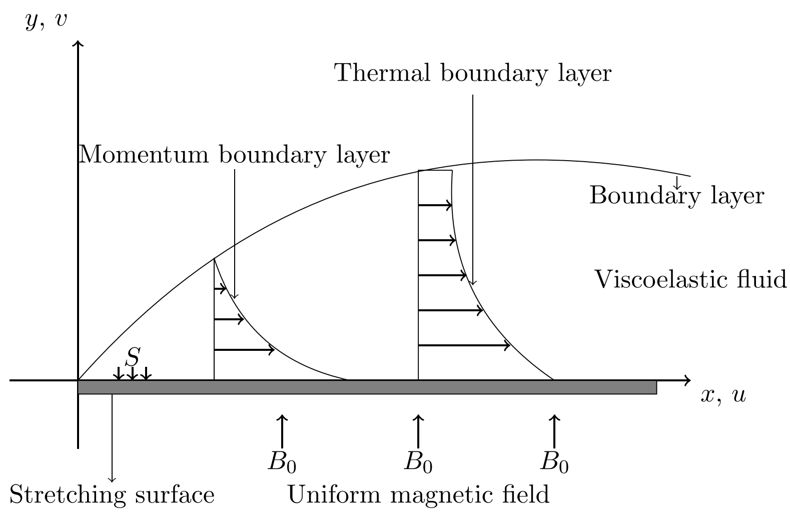

Figure 1. Physical configuration of the problem.

Consider an incompressible upper convected Maxwell fluid flow over a stretching surface in two dimensions. The flow is considered to be steady and laminar. The effect of the magnetic field is included with the Cattaneo - Christov heat flux model in the presence of suction/injection. In this model pressure gradient is negligible. The equations governing the problem under consideration are given by,

$$\frac{\partial u}{\partial x}+\frac{\partial v}{\partial y}=0, \tag{2}$$

$$u\frac{\partial u}{\partial x}+v\frac{\partial u}{\partial y}+\lambda_1\left(u^2\frac{\partial^2 u}{\partial x^2}+v^2\frac{\partial^2 u}{\partial y^2}+2uv\frac{\partial^2 u}{\partial x\partial y}\right)=\nu\frac{\partial^2 u}{\partial y^2}-\frac{\sigma B_0^2}{\rho}u, \tag{3}$$

(4)
$$u\frac{\partial T}{\partial x}+v\frac{\partial T}{\partial y}+\frac{\lambda_2}{c_p}\left(u\frac{\partial u}{\partial x}\frac{\partial T}{\partial x}+v\frac{\partial v}{\partial y}\frac{\partial T}{\partial y}+u\frac{\partial v}{\partial x}\frac{\partial T}{\partial y}+v\frac{\partial u}{\partial y}\frac{\partial T}{\partial x}+2uv\frac{\partial^2 T}{\partial x\partial y}\right.$$
$$\left.+u^2\frac{\partial^2 T}{\partial x^2}+v^2\frac{\partial^2 T}{\partial y^2}\right)=\alpha\frac{\partial^2 T}{\partial y^2}+\frac{\sigma B_0^2}{\rho c_p}u^2.$$

The corresponding boundary conditions are

$$u=U_w(x)=ax,\quad v=v_0,\quad T=T_w\quad \text{at}\quad y=0, \tag{5}$$

$$u\to 0,\quad T\to T_\infty\quad \text{as}\quad y\to\infty, \tag{6}$$

where x and y are the directions along and perpendicular to the surface and u and v are the velocity components along the x and y directions respectively. B_0 is the applied uniform magnetic field, σ is the electrical conductivity of the fluid, $\nu=\frac{\mu}{\rho}$ is the kinematic viscosity, μ is the coefficient of viscosity, ρ is the fluid density, λ_1 is the fluid relaxation time, λ_2 is the thermal relaxation time, T is the temperature of Maxwell fluid, $\alpha=\frac{k}{\rho c_p}$ is the thermal diffusivity, k is the thermal conductivity and c_p is the specific heat at constant pressure, v_0 is the velocity due to suction/injection at the wall, a is the stretching rate of the stretching surface, T_w is the temperature at the wall and T_∞ is the ambient fluid temperature.

By using the following similarity transformations,

$$\eta=\sqrt{\frac{a}{\nu}}y,\quad \psi=x\sqrt{\nu a}f(\eta),\quad \theta=\frac{T-T_\infty}{T_w-T_\infty}, \tag{7}$$

in which ψ is the stream function, the governing partial differential equations (2)-(4) along with the boundary conditions (5)-(6) can be converted to a system of two nonlinear coupled ordinary differential equations,

(8)
$$f'''(\eta)-f'^2(\eta)+f(\eta)f''(\eta)+\beta\left[2f(\eta)f'(\eta)f''(\eta)-f^2(\eta)f'''(\eta)\right]-\mathrm{Mn}f'(\eta)=0,$$

$$\frac{1}{\mathrm{Pr}}\theta''(\eta)+f(\eta)\theta'(\eta)-\gamma\left[f(\eta)f'(\eta)\theta'(\eta)+f^2(\eta)\theta''(\eta)\right]+\mathrm{MnEc}f'^2(\eta)=0, \tag{9}$$

with the boundary conditions,

$$f(\eta)=\mathrm{S},\quad f'(\eta)=1,\quad \theta(\eta)=1\quad \text{at}\quad \eta=0, \tag{10}$$

$$f'(\eta)\to 0,\quad \theta(\eta)\to 0\quad \text{as}\quad \eta\to\infty, \tag{11}$$

where f and θ are the dimensionless stream and temperature functions respectively and the prime denotes the derivative with respect to η. $\mathrm{Mn} = \frac{\sigma B_0^2}{a\rho}$ is the magnetic parameter (Hartmann number), $\mathrm{Ec} = \frac{a^2x^2}{\Delta T c_p}$ is the local Eckert number, $\mathrm{Pr} = \frac{\nu}{\alpha}$ is the Prandtl number, $\beta = \lambda_1 a$ is the elasticity parameter (Deborah number) and $\gamma = \frac{\lambda_2 a}{c_p}$ is the non-dimensional thermal relaxation time, a is a positive constant, $\mathrm{S} = -\frac{v_0}{\sqrt{a\nu}}$ is a suction parameter, $\mathrm{S} > 0$ corresponds to suction, $\mathrm{S} < 0$ correspond to injection and $\mathrm{S} = 0$ is an impermeable surface.

3.1. **Skin friction coefficient.** For the viscoelastic fluid past a stretching surface, the required skin friction is the skin friction coefficient or frictional drag coefficient C_f and is given by,

$$C_f = \frac{\tau_w}{\frac{1}{2}\rho U_w^2}, \tag{12}$$

where $\tau_w = \mu \frac{\partial u}{\partial y}|_{y=0}$ is the surface shear stress or the skin friction along the stretching surface. Thus, we have $\frac{1}{2} C_f \mathrm{Re_x}^{\frac{1}{2}} = f''(0)$ where $\mathrm{Re_x} = \frac{U_w x}{\nu}$ is the local Reynolds number.

3.2. **Wall temperature gradient.** The heat transfer phenomenon is analyzed in terms of dimensionless number of temperature gradient, known as Nusselt number. The local Nusselt number $\mathrm{Nu_x}$ in the present case is derived as,

$$\mathrm{Nu_x} = -\frac{x}{(T_w - T_\infty)} \left(\frac{\partial T}{\partial y}\right)_{y=0}. \tag{13}$$

Thus, we have $\frac{\mathrm{Nu_x}}{\sqrt{\mathrm{Re_x}}} = -\theta'(0)$ where $\mathrm{Re_x} = \frac{U_w x}{\nu}$ is the local Reynolds number.

4. Methodology

The methodology used to solve the problem is Chebyshev wavelet collocation method. In this method, we use shifted Chebyshev wavelets which are defined in 4.1. In 4.1.1, we define finite sum of Chebyshev wavelets for an unknown function.

4.1. **Shifted Chebyshev Wavelets.** The family of Shifted Chebyshev wavelets [62] are defined on the interval $[0, L]$ as,

$$\psi_i(x) = \psi_{n,m}(x) = \begin{cases} \frac{\alpha_m 2^{\frac{\mathcal{K}}{2}}}{\sqrt{L\pi}} T_m\left(\frac{2^{\mathcal{K}}}{L}x - 2n + 1\right), & \xi_1 \leq x \leq \xi_2 \\ 0, & \text{otherwise} \end{cases} \tag{14}$$

where

$$\alpha_m = \begin{cases} \sqrt{2} & m = 0 \\ 2, & m > 0 \end{cases}, \quad \xi_1 = \left(\frac{n-1}{2^{\mathcal{K}-1}}\right) L, \quad \xi_2 = \left(\frac{n}{2^{\mathcal{K}-1}}\right) L. \tag{15}$$

In the above definition, $i = n + 2^{\mathcal{K}-1}m$, $\mathcal{K}$ is the level of resolution, $n = 1, 2, \cdots 2^{\mathcal{K}-1}$ is the translation parameter, $m = 0, 1, 2, \cdots, M-1$, $M > 0$ and x is the normalized time. $T_m(x)$ are Chebyshev polynomials of first-kind of degree m which are orthogonal with respect to the weight function $\omega(x) = \frac{1}{\sqrt{1-x^2}}$ on $[-1, 1]$.

The wavelet collocation points are defined as

$$x_j = \frac{j - 0.5}{N}, \forall j = 1, 2, \cdots, N,$$

where $N = 2^{\mathcal{K}-1}M$.
To solve the differential equations of higher order, we require the following integrals.

$$p_i(x) = \int_0^x \psi_i(x)dx, \quad q_i(x) = \int_0^x p_i(x)dx \quad \text{and} \quad r_i(x) = \int_0^x q_i(x)dx.$$

4.1.1. *Function Approximation.* A function $f(x)$ which is square integrable on $[0, 1)$ can be expressed as infinite sum of Chebyshev wavelets as [56],

$$f(x) = \sum_{n=1}^{\infty}\sum_{m=0}^{\infty} a_{nm}\psi_{nm}(x), \tag{16}$$

where

$$a_{nm} = \int_0^1 f(x)\psi_{nm}(x)\omega_n(x)dx. \tag{17}$$

If the function $f(x)$ is approximated as piece-wise constant in each sub-interval, then equation (16) becomes

$$f(x) = \sum_{n=1}^{2^{\mathcal{K}-1}}\sum_{m=0}^{M-1} a_{nm}\psi_{nm}(x), \tag{18}$$

where a_{nm} are the Chebyshev wavelet coefficients to be determined.

4.2. **Method of Solution.** Using the above defined shifted Chebyshev wavelets and function approximation, the governing nonlinear differential equations are solved. Before that the nonlinearity is reduced by quasilinearization technique as shown below.

Using quasilinearization technique [48, 61, 62] equations (8)-(11) reduce to,
(19)

$$\begin{aligned}
&\Big[1 - \beta f_r^2(\eta)\Big]^2 f'''_{r+1}(\eta) - \Big[\beta f_r^3(\eta) + 2\beta^2 f_r^3(\eta) f_r'(\eta) - f_r(\eta)\Big] \\
&-2\beta f_r(\eta) f_r'(\eta) f''_{r+1}(\eta) - \Big[2f_r'(\eta) - 2\beta f_r(\eta) f_r''(\eta) + \mathrm{Mn} - 2\beta f_r^2(\eta) f_r'(\eta) \\
&+2\beta^2 f_r^3(\eta) f_r''(\eta) - \mathrm{Mn}\beta f_r^2(\eta)\Big] f'_{r+1}(\eta) + \Big[f_r''(\eta) + 2\beta f_r'(\eta) f_r''(\eta) \\
&+2\beta^2 f_r^2(\eta) f_r'(\eta) f_r''(\eta) - 2\beta f_r(\eta) f_r'^2(\eta) - 2\beta \mathrm{Mn} f_r(\eta) f_r'(\eta) \\
&+\beta f_r^2(\eta) f_r''(\eta)\Big] f_{r+1}(\eta) = f_r(\eta) f_r''(\eta) - f_r'^2(\eta) - \beta f_r^2(\eta) f_r'^2(\eta) \\
&+4\beta f_r(\eta) f_r'(\eta) f_r''(\eta) + \beta f_r^3(\eta) f_r''(\eta) - 2\beta \mathrm{Mn} f_r^2(\eta) f_r'(\eta),
\end{aligned}$$

(20)
$$\begin{aligned}&\left[1-\Pr\gamma f_r^2(\eta)\right]^2\theta''_{r+1}(\eta)-\Big[\Pr\gamma f_r(\eta)f'_r(\eta)-\Pr f_r(\eta)-\Pr^2\gamma^2 f_r^3(\eta)f'_r(\eta)\\&+\Pr^2\gamma f_r^3(\eta)\Big]\theta'_{r+1}(\eta)-\Big[\Pr\gamma f_r(\eta)\theta'_r(\eta)-\Pr^2\gamma^2 f_r^3(\eta)\theta'_r(\eta)-2\Pr\mathrm{MnEc}f'_r(\eta)\\&+2\Pr^2\gamma\mathrm{MnEc}f_r^2(\eta)f'_r(\eta)\Big]f'_{r+1}(\eta)-\Big[\Pr^2\gamma^2 f_r^2(\eta)f'_r(\eta)\theta'_r(\eta)-\Pr^2\gamma f_r^2(\eta)\theta'_r(\eta)\\&+\Pr\gamma f'_r(\eta)\theta'_r(\eta)-2\gamma\Pr^2\mathrm{MnEc}f_r(\eta)f_r'^2(\eta)-\Pr\theta'_r(\eta)\Big]f_{r+1}(\eta)=\Pr f_r(\eta)\theta'_r(\eta)\\&+\Pr^2\gamma f_r^3(\eta)\theta'_r(\eta)+\Pr^2\gamma\mathrm{MnEc}f_r^2(\eta)f_r'^2(\eta)-2\Pr\gamma\theta'_r(\eta)f_r(\eta)f'_r(\eta)\\&+\Pr\mathrm{MnEc}f_r'^2(\eta),\end{aligned}$$

(21)
$$\begin{aligned}f_{r+1}(\eta)=\mathrm{S},\quad f'_{r+1}(\eta)=1,\quad \theta_{r+1}(\eta)=1\quad \text{at}\quad \eta=0,\\ f'_{r+1}(\eta)\to 0,\quad \theta_{r+1}(\eta)\to 0\quad \text{as}\quad \eta\to\infty,\end{aligned}$$

where r is the iteration parameter.
Now, equations (19)-(20) are solved using Chebyshev wavelet collocation method. The Chebyshev wavelet series for the highest order derivative can be written as follows:

$$f'''_{r+1}(\eta)=\sum_{i=1}^{N}a_i\psi_i(\eta), \tag{22}$$

$$\theta''_{r+1}(\eta)=\sum_{i=1}^{N}b_i\psi_i(\eta). \tag{23}$$

Integrating equations (22)-(23), then using boundary conditions (21) we obtain the lower order derivatives as

$$f''_{r+1}(\eta)=\sum_{i=1}^{N}a_i\left(p_i(\eta)-\frac{1}{L}q_i(L)\right)-\frac{1}{L}, \tag{24}$$

$$f'_{r+1}(\eta)=\sum_{i=1}^{N}a_i\left(q_i(\eta)-\frac{\eta}{L}q_i(L)\right)+\frac{L-\eta}{L}, \tag{25}$$

$$f_{r+1}(\eta)=\sum_{i=1}^{N}a_i\left(r_i(\eta)-\frac{\eta^2}{2L}q_i(L)\right)+\frac{\eta(2L-\eta)}{2L}+\mathrm{S}, \tag{26}$$

$$\theta'_{r+1}(\eta)=\sum_{i=1}^{N}b_i\left(p_i(\eta)-\frac{1}{L}q_i(L)\right)-\frac{1}{L}, \tag{27}$$

$$\theta_{r+1}(\eta)=\sum_{i=1}^{N}b_i\left(q_i(\eta)-\frac{\eta}{L}q_i(L)\right)+\frac{L-\eta}{L}, \tag{28}$$

where L is sufficiently large number. Substituting equations (22)-(28) and by discretizing equations (19)-(20) using the collocation points $\eta_j=\dfrac{j-0.5}{N}$, $j=1,2,...,N$, we obtain the following system of linear algebraic equations,

$$\sum_{i=1}^{N}a_iS_1=T_1, \tag{29}$$

$$\sum_{i=1}^{N} a_i S_2 + \sum_{i=1}^{N} b_i S_3 = T_2, \tag{30}$$

where

$$\begin{aligned}
S_1 =& \Big[1-\beta f_r^2(\eta)\Big]^2 \psi_i(\eta) - \Big[-f_r(\eta) - 2\beta f_r(\eta) f_r'(\eta) + 2\beta^2 f_r^3(\eta) f_r'(\eta) \\
&+ \beta f_r^3(\eta)\Big]\Big[p_i(\eta) - \frac{1}{L} q_i(L)\Big] - \Big[2f_r'(\eta) - 2\beta f_r(\eta) f_r''(\eta) - 2\beta f_r^2(\eta) f_r'(\eta) \\
&+ \mathrm{Mn} + 2\beta^2 f_r^3(\eta) f_r''(\eta) - \mathrm{Mn}\beta f_r^2(\eta)\Big]\Big[q_i(\eta) - \eta q_i(L)\Big] + \Big[2\beta f_r'(\eta) f_r''(\eta) \\
&- 2\beta \mathrm{Mn} f_r(\eta) f_r'(\eta) + \beta f_r^2(\eta) f_r''(\eta) + 2\beta^2 f_r^2(\eta) f_r'(\eta) f_r''(\eta) + f_r''(\eta) \\
&- 2\beta f_r(\eta) f_r'^2(\eta)\Big]\Big[r_i(\eta) - \frac{\eta^2}{2} q_i(L)\Big], \\
S_2 =& -\Big[\mathrm{Pr}\gamma f_r(\eta)\theta_r'(\eta) - \mathrm{Pr}^2\gamma^2 f_r^3(\eta)\theta_r'(\eta) + 2\mathrm{Pr}^2\gamma \mathrm{MnEc} f_r^2(\eta) f_r'(\eta) \\
&- 2\mathrm{MnPrEc} f_r'(\eta)\Big]\Big[q_i(\eta) - \frac{\eta}{L} q_i(L)\Big] - \Big[\mathrm{Pr}^2\gamma^2 f_r^2(\eta) f_r'(\eta)\theta_r'(\eta) \\
&- \mathrm{Pr}^2\gamma f_r^2(\eta)\theta_r'(\eta) + \mathrm{Pr}\gamma f_r'(\eta)\theta_r'(\eta) - 2\gamma \mathrm{Pr}^2 \mathrm{MnEc} f_r(\eta) f_r'^2(\eta) \\
&- \mathrm{Pr}\theta_r'(\eta)\Big]\Big[r_i(\eta) - \frac{\eta^2}{2L} q_i(L)\Big], \\
S_3 =& \Big[1 - \mathrm{Pr}\gamma f_r^2(\eta)\Big]^2 \psi_i(\eta) - \Big[\mathrm{Pr}\gamma f_r(\eta) f_r'(\eta) - \mathrm{Pr} f_r(\eta) - \mathrm{Pr}^2\gamma^2 f_r^3(\eta) f_r'(\eta) \\
&+ \mathrm{Pr}^2\gamma f_r^3(\eta)\Big]\Big[p_i(\eta) - \frac{1}{L} q_i(L)\Big], \\
T_1 =& \Big[f_r(\eta) f_r''(\eta) - \beta f_r^2(\eta) f_r'^2(\eta) + 4\beta f_r(\eta) f_r'(\eta) f_r''(\eta) - 2\beta \mathrm{Mn} f_r^2(\eta) f_r'(\eta) \\
&+ \beta f_r^3(\eta) f_r''(\eta)\Big] - \Big[\frac{1}{L}\Big]\Big[\beta f_r^3(\eta) + 2\beta^2 f_r^3(\eta) f_r' - 2\beta f_r(\eta) f_r'(\eta) - f_r(\eta)\Big] \\
&+ \Big[\frac{L-\eta}{L}\Big]\Big[2f_r'(\eta) - 2\beta f_r(\eta) f_r''(\eta) - 2\beta f_r^2(\eta) f_r'(\eta) + 2\beta^2 f_r^3(\eta) f_r''(\eta) \\
&+ \mathrm{Mn} - \mathrm{Mn}\beta f_r^2(\eta)\Big] - \Big[\frac{\eta(2L-\eta)}{2L} + \mathrm{S}\Big]\Big[\beta f_r^2(\eta) f_r''(\eta) + 2\beta f_r'(\eta) f_r''(\eta) \\
&+ f_r''(\eta) + 2\beta^2 f_r^2(\eta) f_r'(\eta) f_r''(\eta) - 2\beta f_r(\eta) f_r'^2(\eta) + 2\beta \mathrm{Mn} f_r(\eta) f_r'(\eta)\Big], \\
T_2 =& \Big[\mathrm{Pr}^2\gamma f_r^3(\eta)\theta_r'(\eta) - 2\mathrm{Pr}\gamma\theta_r'(\eta) f_r(\eta) f_r'(\eta) + \mathrm{Pr}^2\gamma \mathrm{MnEc} f_r^2(\eta) f_r'^2(\eta) \\
&+ \mathrm{Pr} f_r(\eta)\theta_r'(\eta) + \mathrm{PrMnEc} f_r'^2(\eta)\Big] - \Big[\frac{1}{L}\Big]\Big[-\mathrm{Pr}^2\gamma^2 f_r^3(\eta) f_r'(\eta) \\
&- \mathrm{Pr} f_r(\eta) + \mathrm{Pr}\gamma f_r(\eta) f_r'(\eta) + \mathrm{Pr}^2\gamma f_r^3(\eta)\Big] + \Big[\frac{L-\eta}{L}\Big]\Big[\mathrm{Pr}\gamma f_r(\eta)\theta_r'(\eta) \\
&- \mathrm{Pr}^2\gamma^2 f_r^3(\eta)\theta_r'(\eta) + 2\mathrm{Pr}^2\gamma \mathrm{MnEc} f_r^2(\eta) f_r'(\eta) - 2\mathrm{MnPrEc} f_r'(\eta)\Big] \\
&+ \Big[\frac{\eta(2L-\eta)}{2L} + \mathrm{S}\Big]\Big[\mathrm{Pr}\gamma f_r'(\eta)\theta_r'(\eta) - \mathrm{Pr}^2\gamma f_r^2(\eta)\theta_r'(\eta) \\
&+ \mathrm{Pr}^2\gamma^2 f_r^2(\eta) f_r'(\eta)\theta_r'(\eta) - \mathrm{Pr}\theta_r'(\eta) - 2\gamma \mathrm{Pr}^2 \mathrm{MnEc} f_r(\eta) f_r'^2(\eta)\Big].
\end{aligned}$$

Quasilinearization is an iterative technique that requires an initial approximation to start the the procedure. Thus, we select an auxiliary linear operator for the governing equations respectively as,

$$L_f = f''' - f' \quad \text{and} \quad L_\theta = \theta'' - \theta. \tag{31}$$

The initial approximations $f_0(\eta)$ and $\theta_0(\eta)$ are obtained from equation (31) using the boundary conditions (21) as,

$$f_0(\eta) = \mathrm{S} + (1 - e^{-\eta}) \quad \text{and} \quad \theta_0(\eta) = e^{-\eta}. \tag{32}$$

Equations (29)-(30) can be solved simultaneously to obtain the Chebyshev wavelet coefficients a_i and b_i, $\forall\, i = 0, 1, \ldots N$. These coefficients are then substituted in equations (22)-(28) to obtain the approximate solutions at the collocation points $\eta \to \eta_j$. The comparison of numerical solutions obtained by the Chebyshev wavelet collocation method and the Haar wavelet collocation method for $f'(\eta)$ and $\theta(\eta)$ is as shown in Fig. 2a and Fig. 2b respectively. We can see that the Chebyshev wavelet solutions are in good agreement with the Haar wavelet solutions.

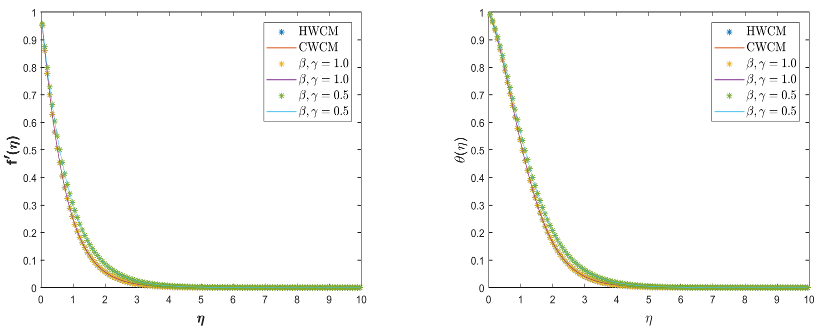

(A) Velocity profile $f'(\eta)$ (B) Temperature profile $\theta(\eta)$

FIGURE 2. Comparison of numerical solutions of $f'(\eta)$ and $\theta(\eta)$ for different values of $\beta, \gamma = 0.5, 1$ when $\mathrm{Pr} = \mathrm{Ec} = \mathrm{Mn} = 1, \mathrm{S} = 0$.

The important dimensionless physical parameters $f''(0)$ and $\theta'(0)$ are determined numerically from equations (8)-(11) using the Chebyshev wavelet collocation method as,

$$f''(0) = -\frac{1}{L} - \frac{1}{L}\sum_{i=1}^{N} a_i q_i(L), \tag{33}$$

$$\theta'(0) = -\frac{1}{L} - \frac{1}{L}\sum_{i=1}^{N} b_i q_i(L). \tag{34}$$

5. Error Analysis

Using the following lemma through the proofs of Theorem 1 and Theorem 2, the accuracy of the Chebyshev wavelet collocation method is carried out and its convergence is verified.

Lemma 5.1. *Let $f(\eta) \in L^2(\mathbb{R})$ be a continuous function in $(0, L)$ with $|f''(\eta)| \leq K_1$; $\forall\, \eta \in (0,1)$; $K_1 > 0$. If $f(\eta) = \sum_{n=1}^{\infty}\sum_{m=0}^{\infty} a_{nm}\psi_{nm}(\eta)$, then the convergence of the series is uniform.*

Proof. Consider,

$$a_{nm} = \langle f(\eta), \psi_{n,m}(\eta)\rangle_{L^2_\omega[0,1)} = \int_0^1 f(\eta)\psi_{n,m}(\eta)\omega_n(\eta)d\eta$$
$$= \int_{\left(\frac{n-1}{2^{\mathcal{K}-1}}\right)L}^{\left(\frac{n}{2^{\mathcal{K}-1}}\right)L} \frac{\alpha_m}{\sqrt{L\pi}} 2^{\frac{\mathcal{K}}{2}} f(\eta) T_m\left(\frac{2^{\mathcal{K}}\eta}{L} - 2n + 1\right)\omega\left(\frac{2^{\mathcal{K}}\eta}{L} - 2n + 1\right)d\eta.$$

For $m > 1$, we have

$$a_{nm} = \int_\pi^0 \frac{2}{\sqrt{L\pi}} 2^{\frac{\mathcal{K}}{2}} f\left(\frac{L(\cos\theta + 2n - 1)}{2^{\mathcal{K}}}\right)\cos(m\theta)\frac{1}{\sin\theta}\left(-\frac{L\sin\theta}{2^{\mathcal{K}}}\right)d\theta$$
$$= \frac{2}{2^{\frac{\mathcal{K}}{2}}}\sqrt{\frac{L}{\pi}}\int_0^\pi f\left(\frac{L(\cos\theta + 2n - 1)}{2^{\mathcal{K}}}\right)\cos(m\theta)d\theta$$
$$= \frac{L^2}{2^{\frac{5\mathcal{K}}{2}}m}\sqrt{\frac{L}{\pi}}\int_0^\pi f''\left(\frac{L(\cos\theta + 2n - 1)}{2^{\mathcal{K}}}\right)\sin\theta\left[\frac{\sin(m-1)\theta}{m-1} - \frac{\sin(m+1)\theta}{m+1}\right]d\theta.$$

Since $|f''(t)| \leq K_1$, we have

(35)
$$|a_{nm}| \leq \frac{K_1 L^{\frac{5}{2}}}{2^{\frac{5\mathcal{K}}{2}} m\sqrt{\pi}}\int_0^\pi \left|\sin\theta\left[\frac{\sin(m-1)\theta}{m-1} - \frac{\sin(m+1)\theta}{m+1}\right]\right|d\theta \leq \frac{2\sqrt{\pi}K_1 L^{\frac{5}{2}}}{2^{\frac{5\mathcal{K}}{2}}(m^2-1)}.$$

Since $n \leq 2^{\mathcal{K}-1}$, equation (35) becomes

$$|a_{nm}| < \left(\frac{L}{2n}\right)^{\frac{5}{2}}\frac{2\sqrt{\pi}K_1}{(m^2-1)}. \tag{36}$$

For $m = 1$, we have

$$a_{nm} = \sqrt{\frac{L}{\pi}}\frac{2}{2^{\frac{\mathcal{K}}{2}}}\int_0^\pi f\left(\frac{L(\cos(\theta) + 2n - 1)}{2^{\mathcal{K}}}\right)\cos(\theta)d\theta \tag{37}$$
$$= \sqrt{\frac{L}{\pi}}\frac{2L}{2^{\frac{3\mathcal{K}}{2}}}\int_0^\pi f'\left(\frac{L(\cos(\theta) + 2n - 1)}{2^{\mathcal{K}}}\right)\sin^2(\theta)d\theta. \tag{38}$$

Note that $f'(\eta)$ is bounded on $[0, L]$ due to the fact that $|f''(t)| \leq K_1$ and from mean value theorem. If $|f'(\eta)| \leq K_2$; $K_2 > 0$. Then,

(39)
$$|a_{nm}| \leq \sqrt{\frac{L}{\pi}}\frac{2L}{2^{\frac{3\mathcal{K}}{2}}}\int_0^\pi \left|f'\left(\frac{L(\cos(\theta) + 2n - 1)}{2^{\mathcal{K}}}\right)\sin^2(\theta)\right|d\theta \leq \left(\frac{L}{2^{\mathcal{K}}}\right)^{\frac{3}{2}}\sqrt{\pi}K_2.$$

Since $n \leq 2^{\mathcal{K}-1}$, equation (35) becomes

$$|a_{nm}| < \left(\frac{L}{2n}\right)^{\frac{3}{2}}\sqrt{\pi}K_2. \tag{40}$$

The relations (36) and (40) are absolutely convergent. For $m = 0$, according to the definition of $\psi_{nm}(\eta)$ in equation (14), the series $\sum_{n=1}^{\infty} a_{n0}\psi_{n0}(\eta)$ is convergent. Therefore, the series $\sum_{n=1}^{\infty}\sum_{m=0}^{\infty} a_{nm}\psi_{nm}(\eta)$ converges to $f(\eta)$ uniformly. □

Now, we introduce Theorem 1 and Theorem 2, which gives an upper estimate for the truncation error.

Theorem 5.2. *If $f(\eta)$ is the exact solution and $f_N(\eta)$ is the Chebyshev wavelet solution for the velocity profile, then*

$$||E_{1_N}|| \leq \frac{\sqrt{C_1\pi}K_1 L^{\frac{5}{2}}}{2^{\frac{3}{2}}}\left(\sum_{n=2^{\mathcal{K}-1}+1}^{\infty}\frac{1}{n^5}\sum_{m=M}^{\infty}\frac{1}{(m^2-1)^2}\right)^{\frac{1}{2}}.$$

Proof. From equation (26), we have

$$f_N(\eta) = \sum_{i=1}^{N} a_i\left(r_i(\eta) - \frac{\eta^2}{2L}q_i(L)\right) + \left(\frac{\eta(2L-\eta)}{2L}\right) + \text{S}. \tag{41}$$

Taking the asymptotic expansion of the equation (48), we obtain

$$f(\eta) = \sum_{i=1}^{\infty} a_i\left(r_i(\eta) - \frac{\eta^2}{2L}q_i(L)\right) + \left(\frac{\eta(2L-\eta)}{2L}\right) + \text{S}. \tag{42}$$

The error estimate is given by,

$$\begin{aligned}||E_{1_N}|| &= ||f(\eta) - f_N(\eta)||\\ &= \left|\sum_{i=N+1}^{\infty} a_i\left(r_i(\eta) - \frac{\eta^2}{2L}q_i(L)\right)\right|.\end{aligned}$$

We have,

$$\begin{aligned}||E_{1_N}||^2 &= \left|\int_{-\infty}^{\infty}\left\langle\sum_{i=N+1}^{\infty} a_i\left(r_i(\eta) - \frac{\eta^2}{2L}q_i(L)\right), \sum_{l=N+1}^{\infty} a_l\left(r_l(\eta)\right.\right.\right.\\ &\qquad\left.\left.\left. - \frac{\eta^2}{2L}q_l(L)\right)\right\rangle d\eta\right|\\ &= \left|\sum_{i=N+1}^{\infty} a_i \sum_{l=N+1}^{\infty} a_l \int_0^1 \left(r_i(\eta) - \frac{\eta^2}{2L}q_i(L)\right)\left(r_l(\eta) - \frac{\eta^2}{2L}q_l(L)\right) d\eta\right|\\ &\leq \sum_{i=N+1}^{\infty}\sum_{l=N+1}^{\infty} |a_i|\,|a_l|\, C_1\end{aligned}$$

where

$$C_1 = \sup_{i,l}\int_0^1 \left(r_i(\eta) - \frac{\eta^2}{2L}q_i(L)\right)\left(r_l(\eta) - \frac{\eta^2}{2L}q_l(L)\right) d\eta. \tag{43}$$

Therefore, we obtain

$$||E_{1_N}||^2 \leq C_1 \sum_{i=N+1}^{\infty} |a_i| \sum_{l=N+1}^{\infty} |a_l|. \tag{44}$$

Using the Lemma 5.1, we arrive at

$$\begin{aligned}\sum_{i=N+1}^{\infty}|a_i| &\leq \frac{\sqrt{\pi}K_1L^{\frac{5}{2}}}{2^{\frac{3}{2}}}\sum_{n=2^{\mathcal{K}-1}+1}^{\infty}\sum_{m=M}^{\infty}\frac{1}{n^{\frac{5}{2}}(m^2-1)},\\ \sum_{l=N+1}^{\infty}|a_l| &\leq \frac{\sqrt{\pi}K_1L^{\frac{5}{2}}}{2^{\frac{3}{2}}}\sum_{n=2^{\mathcal{K}-1}+1}^{\infty}\sum_{m=M}^{\infty}\frac{1}{n^{\frac{5}{2}}(m^2-1)}.\end{aligned} \tag{45}$$

Finally, we get

$$||E_{1_N}||^2 \leq \frac{C_1\pi K_1^2L^5}{8}\sum_{n=2^{\mathcal{K}-1}+1}^{\infty}\sum_{m=M}^{\infty}\frac{1}{n^5(m^2-1)^2}. \tag{46}$$

Therefore,

$$||E_{1_N}|| \leq \frac{\sqrt{C_1\pi}K_1L^{\frac{5}{2}}}{2^{\frac{3}{2}}}\left(\sum_{n=2^{\mathcal{K}-1}+1}^{\infty}\frac{1}{n^5}\sum_{m=M}^{\infty}\frac{1}{(m^2-1)^2}\right)^{\frac{1}{2}}. \tag{47}$$

We observe that $||E_{1_N}|| \to 0$ as $\mathcal{K}, M \to \infty$. Thus, the accuracy of the Chebyshev wavelet method improves as the number of collocation points N increases. □

Theorem 5.3. *If $\theta(\eta)$ is the exact solution and $\theta_N(\eta)$ is the Chebyshev wavelet solution for the temperature profile, then*

$$||E_{2_N}|| \leq \frac{\sqrt{C_2\pi}K_1L^{\frac{5}{2}}}{2^{\frac{3}{2}}}\left(\sum_{n=2^{\mathcal{K}-1}+1}^{\infty}\frac{1}{n^5}\sum_{m=M}^{\infty}\frac{1}{(m^2-1)^2}\right)^{\frac{1}{2}}.$$

Proof. From equation (28), we have

$$\theta_N(\eta) = \sum_{i=1}^{N} b_i\left(q_i(\eta) - \frac{\eta}{L}q_i(L)\right) + \left(\frac{L-\eta}{L}\right). \tag{48}$$

Taking the asymptotic expansion of the equation (48), we obtain

$$\theta(\eta) = \sum_{i=1}^{N} b_i\left(q_i(\eta) - \frac{\eta}{L}q_i(L)\right) + \left(\frac{L-\eta}{L}\right). \tag{49}$$

The error estimate is given by,

$$\begin{aligned}||E_{2_N}|| &= ||\theta(\eta) - \theta_N(\eta)||\\ &= \left|\sum_{i=N+1}^{\infty} b_i\left(q_i(\eta) - \frac{\eta}{L}q_i(L)\right)\right|.\end{aligned}$$

We have,

$$||E_{2_N}||^2 = \left| \int_{-\infty}^{\infty} \left\langle \sum_{i=N+1}^{\infty} b_i \left(q_i(\eta) - \frac{\eta}{L} q_i(L) \right), \sum_{l=N+1}^{\infty} b_l \left(q_l(\eta) - \frac{\eta}{L} q_l(L) \right) \right\rangle d\eta \right|$$

$$= \left| \sum_{i=N+1}^{\infty} b_i \sum_{l=N+1}^{\infty} b_l \int_0^1 \left(q_l(\eta) - \frac{\eta}{L} q_l(L) \right) \left(q_l(\eta) - \frac{\eta}{L} q_l(L) \right) d\eta \right|$$

$$\leq \sum_{i=N+1}^{\infty} \sum_{l=N+1}^{\infty} |b_i|\, |b_l|\, C_2$$

where

$$C_2 = \sup_{i,l} \int_0^1 \left(q_i(\eta) - \frac{\eta}{L} q_i(L) \right) \left(q_l(\eta) - \frac{\eta}{L} q_l(L) \right) d\eta. \tag{50}$$

Therefore, we obtain

$$||E_{2_N}||^2 \leq C_2 \sum_{i=N+1}^{\infty} |b_i| \sum_{l=N+1}^{\infty} |b_l| . \tag{51}$$

Using the Lemma 5.1, we arrive at

$$\begin{aligned} \sum_{i=N+1}^{\infty} |b_i| &\leq \frac{\sqrt{\pi} K_1 L^{\frac{5}{2}}}{2^{\frac{3}{2}}} \sum_{n=2^{\mathcal{K}-1}+1}^{\infty} \sum_{m=M}^{\infty} \frac{1}{n^{\frac{5}{2}}(m^2-1)}, \\ \sum_{l=N+1}^{\infty} |b_l| &\leq \frac{\sqrt{\pi} K_1 L^{\frac{5}{2}}}{2^{\frac{3}{2}}} \sum_{n=2^{\mathcal{K}-1}+1}^{\infty} \sum_{m=M}^{\infty} \frac{1}{n^{\frac{5}{2}}(m^2-1)}. \end{aligned} \tag{52}$$

Finally, we get

$$||E_{2_N}||^2 \leq \frac{C_2 \pi K_1^2 L^5}{8} \sum_{n=2^{\mathcal{K}-1}+1}^{\infty} \sum_{m=M}^{\infty} \frac{1}{n^5 (m^2-1)^2}. \tag{53}$$

Therefore,

$$||E_{2_N}|| \leq \frac{\sqrt{C_2 \pi} K_1 L^{\frac{5}{2}}}{2^{\frac{3}{2}}} \left(\sum_{n=2^{\mathcal{K}-1}+1}^{\infty} \frac{1}{n^5} \sum_{m=M}^{\infty} \frac{1}{(m^2-1)^2} \right)^{\frac{1}{2}}. \tag{54}$$

We observe that $||E_{2_N}|| \to 0$ as $\mathcal{K}, M \to \infty$. Thus, the accuracy of the Chebyshev wavelet method improves as the number of collocation points N increases. □

6. Results and Discussion

We have considered the heat transfer and boundary layer flow of an upper convected Maxwell fluid over a stretching surface. We employ Cattaneo - Christov heat flux model to analyze the heat transfer process. The solutions of transformed momentum and energy equation along with boundary conditions are obtained by means of Chebyshev wavelet collocation method. To solve and analyze this analysis, we have used Matlab software to facilitate the process. The velocity and temperature profiles have been obtained using

128 ($\mathcal{K} = 5$, $M = 8$) collocation points.

TABLE 1. The values of $-f''(0)$ and $-\theta'(0)$ when S = 0.

β	γ	Pr	Mn	Ec	$-f''(0)$	$-\theta'(0)$
0.1					1.026189	0.184191
0.2					1.051893	0.186769
0.5	0.2	1.0	1.0	1.0	1.126236	0.191226
0.8					1.196711	0.192470
1.0					1.241748	0.192221
	0.0				1.051893	0.171139
	0.2				1.051893	0.186769
0.2	0.5	1.0	1.0	1.0	1.051893	0.213079
	0.8				1.051893	0.243091
	1.0				1.051893	0.265262
		0.5			1.051893	0.140159
0.2	0.2	1.0	1.0	1.0	1.051893	0.186769
		2.0			1.051893	0.197212
		3.0			1.051893	0.159070
			0.2		1.051893	0.503436
0.2	0.2	1.0	0.6	1.0	1.051893	0.345103
			1.0		1.051893	0.186769
			1.5		1.051893	−0.011148
				0.2	1.051893	0.503436
0.2	0.2	1.0	1.0	0.6	1.051893	0.345103
				1.0	1.051893	0.186769
				1.5	1.051893	−0.011148

In Table 1, we have listed the skin friction coefficient for no suction flow, where we observe prominently that the variation of viscoelastic parameter β shows the variation in skin friction coefficient whereas, variation in other parameters such as γ, Pr, Mn and Ec does not affect the skin friction coefficient. At the same time, wall temperature gradient shows variations in β along with the variations in γ, Pr, Mn and Ec.

TABLE 2. Comparison of local Nusselt number $-\theta'(0)$ in the case of Newtonian fluid ($\beta = \gamma = a = S = 0$) for different values of Pr.

Pr	Wang [63]	Gorla [64]	Khan [65]	Malik [66]	Siri(HWCM) [22]	Siri(RK GILL) [22]	Present results
0.70	0.4539	0.5349	0.4539	0.45392	0.453930	0.453917	0.454447
2.00	0.9114	0.9114	0.9113	0.91135	0.911345	0.911358	0.911353
7.00	1.8954	1.8905	1.8954	1.89543	1.895489	1.895403	1.895400
20.0	3.3539	3.3539	3.3539	3.35395	3.353905	3.353904	3.353902

The observation in Table 2 reveals the following: For higher values of Pr, the limiting case of present problem exactly matches with Khan [65], Malik [66] and Siri [22] upto 4 decimal places for $\mathcal{K} = 5$, $M = 18$ and

$L = 10$. Whereas for small values of Pr we get, matching result for present problem to previous scientist for lesser collocation points. Thus, when the viscosity increases, we need more collocation points for converging solutions.

TABLE 3. The values of $-f''(0)$ when $\mathrm{Pr} = 1$ and $S = 0$.

γ	$-f''(0)$								
	$\beta = 0.1$			$\beta = 0.15$			$\beta = 0.2$		
	Siri [22]		Present results	Siri [22]		Present results	Siri [22]		Present results
	RK GILL	HWQM	CWCM	RK GILL	HWQM	CWCM	RK GILL	HWQM	CWCM
0.1	1.02654	1.02653	1.02653	1.03940	1.03939	1.03939	1.05215	1.05214	1.05214
0.4	1.02654	1.02653	1.02653	1.03940	1.03939	1.03939	1.05215	1.05214	1.05214
0.5	1.02654	1.02653	1.02653	1.03940	1.03939	1.03939	1.05215	1.05214	1.05214
0.6	1.02654	1.02653	1.02653	1.03940	1.03939	1.03939	1.05215	1.05214	1.05214
0.8	1.02654	1.02653	1.02653	1.03940	1.03939	1.03939	1.05215	1.05214	1.05214
1.0	1.02654	1.02653	1.02653	1.03940	1.03939	1.03939	1.05215	1.05214	1.05214

TABLE 4. The values of $-\theta'(0)$ when $\mathrm{Pr} = 1$ and $S = 0$.

γ	$-\theta'(0)$								
	$\beta = 0.1$			$\beta = 0.15$			$\beta = 0.2$		
	Siri [22]		Present results	Siri [22]		Present results	Siri [22]		Present results
	RK GILL	HWQM	CWCM	RK GILL	HWQM	CWCM	RK GILL	HWQM	CWCM
0.1	0.58379	0.58379	0.58379	0.57983	0.57983	0.57983	0.57593	0.57593	0.57593
0.4	0.61014	0.61014	0.61014	0.60553	0.60554	0.60554	0.60101	0.60101	0.60101
0.5	0.61998	0.61998	0.61998	0.61516	0.61516	0.61516	0.61042	0.61042	0.61042
0.6	0.63029	0.63029	0.63029	0.62526	0.62526	0.62526	0.62031	0.62031	0.62031
0.8	0.65215	0.65215	0.65215	0.64673	0.64673	0.64673	0.64138	0.64138	0.64138
1.0	0.67551	0.67551	0.67551	0.66972	0.66972	0.66972	0.66400	0.66400	0.66400

In Tables 3 and 4, we have shown that our values match with the values of Siri [22] in the limiting case $\mathrm{Mn} = 0$. Table 3 shows upto 5 digit matching for less elasticity and for higher values of elasticity. In Table 4, for lesser values of γ as well as for higher values of γ it matches upto 5 digits.

Table 5 displays the values of skin friction coefficient and Table 6 shows the wall temperature gradient values for different values of S and β in comparison with the values of Siri [22]. It is clear from the Table 5 and Table 6 that the values of $-f''(0)$ and $-\theta'(0)$ are increases (in the absolute sense) as the value of S increases.

The effect of elasticity on velocity and temperature profiles are shown in Figs. 3 and 4. The elastic force disappears and fluid becomes the Newtonian fluid if $\beta = 0$. Fluid shows purely viscous behaviour for a smaller elasticity number i.e., for $\beta < 1$ whereas fluid acts as a elastically solid material for $\beta > 1$. Due to this, for smaller value of β we can see that the larger magnitude of velocity. In Fig. 3, we can see that velocity profile decreases with increase in elasticity number β. That is, for higher values of β the velocity

Table 5. The values of $-f''(0)$ for different values of β and S when Pr = 1 and $\gamma = 0.5$.

S	$\beta = 0.1$			$\beta = 0.15$			$\beta = 0.2$		
	Siri [22]		Present results	Siri [22]		Present results	Siri [22]		Present results
	RK GILL	HWQM	CWCM	RK GILL	HWQM	CWCM	RK GILL	HWQM	CWCM
−1.0	0.59681	0.59764	0.59764	–	0.58640	0.58640	–	0.57485	0.57485
−0.6	0.73250	0.73351	0.73351	0.72619	0.72733	0.72733	0.72004	0.72106	0.72106
−0.3	0.86492	0.86440	0.86440	0.86510	0.86508	0.86508	0.86570	0.86568	0.86568
0.0	1.02654	1.02653	1.02653	1.03940	1.04003	1.04003	1.05215	1.05271	1.05271
0.2	1.15770	1.15770	1.15770	1.18362	1.18361	1.18361	1.21115	1.20962	1.20962
0.3	1.23124	1.23064	1.23064	1.26593	1.26542	1.26542	1.30242	1.30056	1.30056
0.6	1.48751	1.48644	1.48644	1.56384	1.56195	1.56195	–	1.64070	1.64070

Table 6. The values of $-\theta'(0)$ for different values of β and S when Pr = 1 and $\gamma = 0.5$.

S	$\beta = 0.1$			$\beta = 0.15$			$\beta = 0.2$		
	Siri [22]		Present results	Siri [22]		Present results	Siri [22]		Present results
	RK GILL	HWQM	CWCM	RK GILL	HWQM	CWCM	RK GILL	HWQM	CWCM
−1.0	0.14996	0.16047	0.16047	–	0.16116	0.16116	–	0.16186	0.16186
−0.6	0.29747	0.29864	0.29864	0.29721	0.29825	0.29825	0.29673	0.29788	0.29788
−0.3	0.43848	0.43362	0.43362	0.43370	0.43161	0.43161	0.42215	0.42964	0.42964
0.0	0.61998	0.61998	0.61998	0.61516	0.61516	0.61516	0.61042	0.61061	0.61061
0.2	0.79129	0.79129	0.79129	0.78417	0.78417	0.78417	0.77714	0.77715	0.77715
0.3	0.89857	0.89891	0.89891	0.88998	0.89024	0.89024	0.88119	0.88164	0.88164
0.6	1.37559	1.37604	1.37604	1.35999	1.36049	1.36049	–	1.34471	1.34471

in boundary layer increases. Physically, for larger values of β viscous force restricts the fluid motion as a result velocity decreases. Fig. 4 shows variation in fluid temperature with β. As β increases fluid temperature increases and thus elastic force promotes heat transfer of viscoelastic fluid.

Figs. 5 and 6 represents the effect of magnetic field Mn on velocity and temperature profiles. Fig. 5 shows increase in magnetic parameter decreases the velocity profile and the reverse effect is seen for temperature profile in Fig. 6. This is because the increasing value of Mn tends to the increasing of Lorentz force, which produces more resistance to the transport phenomena.

Fig. 7 displays the effect of viscous dissipation parameter which is given by Eckert number Ec on temperature profile. Temperature profile increases with increase in Eckert number. The effect of non-dimensional heat flux relaxation time γ on temperature profile is shown in Fig. 8. Temperature profile decreases and hence the thermal boundary layer thickness decreases due to the increase in γ.

Fig. 9 depicts the temperature profile for different values of Prandtl number Pr. In Fig. 9, we see that increase in Pr decreases the temperature profile. This indicates that the temperature boundary layer is thinner for large Prandtl number. Physically, as Pr grows, thermal diffusivity reduces, resulting in decreased energy penetration ability due to thinner thermal boundary layers. The effect of suction/injection parameter S on velocity and temperature profiles is shown in Fig. 10. For increasing value of S, the velocity and temperature profiles decreases.

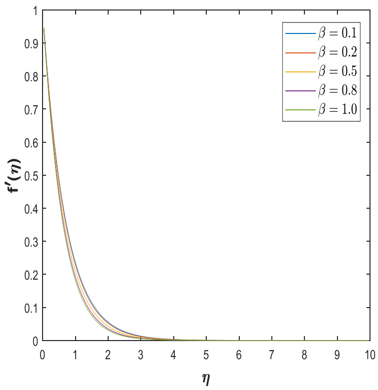

FIGURE 3. Velocity profile for different values of β when $\mathrm{Mn} = 1, \mathrm{S} = 0$.

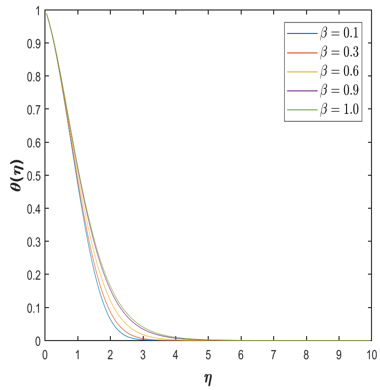

FIGURE 4. Temperature profile for different values of β when $\mathrm{Pr} = \gamma = \mathrm{Ec} = \mathrm{Mn} = 1, \mathrm{S} = 0$.

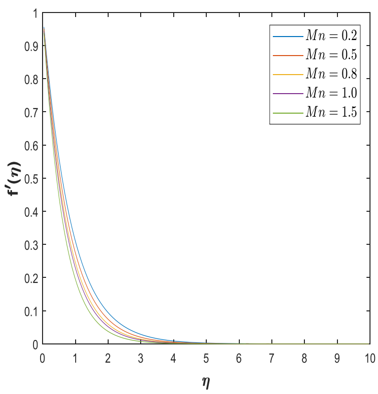

FIGURE 5. Velocity profile for different values of Mn when $\beta = 0.2, \mathrm{S} = 0$.

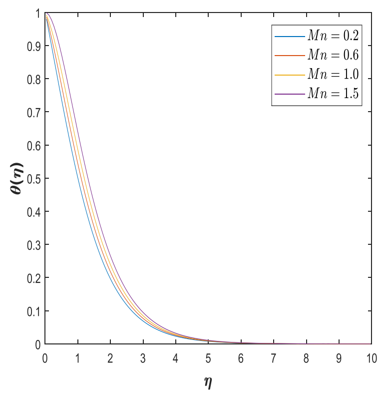

FIGURE 6. Temperature profile for different values of Mn when $\mathrm{Pr} = \mathrm{Ec} = 1, \beta = \gamma = 0.2, \mathrm{S} = 0$.

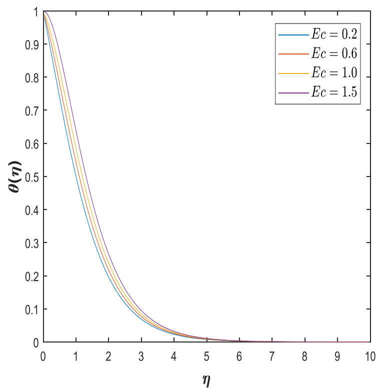

FIGURE 7. Temperature profile for different values of Ec when $\mathrm{Pr} = \mathrm{Mn} = 1, \beta = \gamma = 0.2, \mathrm{S} = 0$.

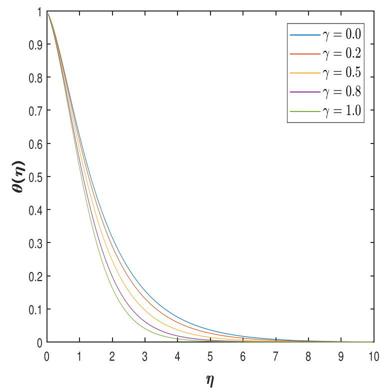

FIGURE 8. Temperature profile for different values of γ when $\mathrm{Pr} = \mathrm{Ec} = \mathrm{Mn} = \beta = 1, \mathrm{S} = 0$.

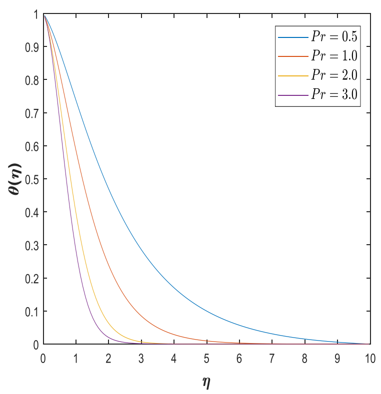

FIGURE 9. Temperature profile for different values of Pr when $\mathrm{Ec} = \mathrm{Mn} = 1, \beta = \gamma = 0.2, \mathrm{S} = 0$.

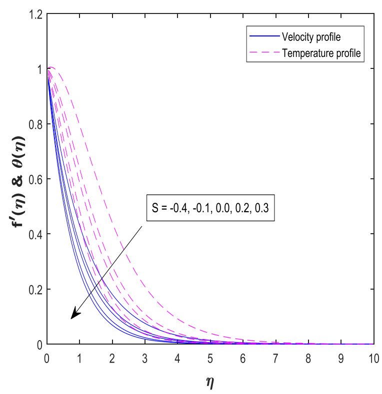

FIGURE 10. Temperature and velocity profiles for different values of S when $\mathrm{Pr} = \mathrm{Mn} = \mathrm{Ec} = 1, \beta = \gamma = 0.2$.

7. CONCLUSION

The study of boundary layer flow and heat transfer of an upper convected Maxwell fluid past a stretching surface in the presence of suction/injection has been carried out in this work. The partial differential equations governing the system are reduced to a set of ordinary differential equations along with the boundary conditions using similarity transformations. The solution of resultant equations is obtained numerically by the Chebyshev wavelet collocation method. The effect of physical parameters such as Deborah number

β, non-dimensional thermal relaxation time γ, suction/injection parameter S, Prandtl number Pr, Hartmann number Mn and Eckert number Ec is analyzed. Following are the important findings of current study.

- The Deborah number β has the opposite effect on the velocity and temperature profiles.
- The effect of the magnetic field Mn is the same as that of the Deborah number β i.e., Mn decreases the velocity profile and has the opposite effect on the temperature profile.
- As the value of Prandtl number Pr increases, the temperature profile decreases and hence thermal boundary layer becomes thinner.
- Both velocity and temperature profiles are affected by variation in suction/injection parameter S. There is a reduction in velocity and temperature profiles for a large value of S.
- Increasing value of suction/injection parameter S, increases (in the absolute sense) the value of $f''(0)$.
- Variation of heat flux relaxation γ has no effect on surface friction coefficient $f''(0)$.
- The increasing value of heat flux relaxation γ increases (in the absolute sense) the wall temperature gradient $\theta'(0)$ whereas the increasing value of Deborah number β decreases (in the absolute sense) the wall temperature gradient $\theta'(0)$.

References

[1] R.K. Rathy, *An introduction to fluid dynamics.* OXFORD & IBH PUBLISHING CO. (1976).

[2] F. Olsson, & J. Ystrom, *Some properties of the upper convected Maxwell model for viscoelastic fluid flow*, J. Nonnewton. Fluid Mech. 48(1-2) (1993), 125-145. https://doi.org/10.1016/0377-0257(93)80068-M.

[3] K. Sadeghy, A.H. Najafi, & M. Saffaripour, *Sakiadis flow of an upper-convected Maxwell fluid*, Int J Non Linear Mech. 40(9) (2005), 1220-1228. https://doi.org/10.1016/j.ijnonlinmec.2005.05.006.

[4] Z. Abbas, M. Sajid, & T. Hayat, *MHD boundary-layer flow of an upper-convected Maxwell fluid in a porous channel*, Theor Comput Fluid Dyn. 20 (2006), 229-238. https://doi.org/10.1007/s00162-006-0025-y.

[5] T. Hayat, Z. Abbas, & M. Sajid, *Series solution for the upper-convected Maxwell fluid over a porous stretching plate*, Phys. Lett. A. 358(5-6) (2006), 396-403. https://doi.org/10.1016/j.physleta.2006.04.117.

[6] T. Hayat, Z. Abbas, & N. Ali, *MHD flow and mass transfer of a upper-convected Maxwell fluid past a porous shrinking sheet with chemical reaction species*, Phys. Lett. A 372(26) (2008), 4698-4704. https://doi.org/10.1016/j.physleta.2008.05.006.

[7] T. Hayat, Z. Abbas, & M. Sajid, *MHD stagnation-point flow of an upper-convected Maxwell fluid over a stretching surface*, Chaos Solit. Fractals. 39(2) (2009), 840-848. https://doi.org/10.1016/j.chaos.2007.01.067.

[8] T. Hayat, & Z. Abbas, *Channel flow of a Maxwell fluid with chemical reaction*, Z. fur Angew. Math. Phys. 59 (2008), 124-144. https://doi.org/10.1007/s00033-007-6067-115.

[9] T. Hayat, M. Mustafa, & S. Mesloub, *Mixed convection boundary layer flow over a stretching surface filled with a Maxwell fluid in presence of Soret and Dufour effects*, Z. Naturforsch. A. 65(5) (2010), 401-410. https://doi.org/10.1515/zna-2010-0505.

[10] T. Hayat, R. Sajjad, Z. Abbas, M. Sajid, & A.A. Hendi, *Radiation effects on MHD flow of Maxwell fluid in a channel with porous medium*, Int. J. Heat Mass Transf. 54(4) (2011), 854-862. https://doi.org/10.1016/j.ijheatmasstransfer.2010.09.069.

[11] T. Hayat, Z. Iqbal, M. Mustafa, & A. Alsaedi, *Momentum and heat transfer of an upper-convected Maxwell fluid over a moving surface with convective boundary conditions*, Nucl. Eng. Des. 252 (2012), 242-247. https://doi.org/10.1016/j.nucengdes.2012.07.012.

[12] D. Tripathi, S.K. Pandey, & S. Das, *Peristaltic flow of viscoelastic fluid with fractional Maxwell model through a channel*, Appl. Math. Comput. 215(10) (2010), 3645-3654. https://doi.org/10.1016/j.amc.2009.11.002.

[13] H. Chaudhary, D. Sunil, & V.N. Mishra, *Effects of variable viscosity and thermal conductivity on MHD flow due to the permeable moving plate*, Stoch. Model. Appl. 25(2) (2021), 271-288. https://www.researchgate.net/publication/362468221.

[14] H. Chaudhary, D. Sunil, & V.N. Mishra, *Boundary layer flow over a moving in a nanofluid with viscous dissipation in a saturated porous media*, Stoch. Model. Appl. 26(1) (2022), 103-177. https://www.mukpublications.com/resources/13_himanshu.pdf.

[15] H.R. Marasi, V.N. Mishra, & M. Daneshbastam, *A constructive approach for solving system of fractional differential equations*, Wavelets Fractal Ana. 3 (2017), 40-47. https://doi.org/10.1515/wwfaa-2017-0004.

[16] N.T. Negero, G.F. Duressa, L. Rathour, & V.N. Mishra, *A novel fitted numerical scheme for singularly perturbed delay parabolic problems with two small parameters*, Partial Differ. Equ. Appl. Math. 8 (2023), 100546. https://doi.org/10.1016/j.padiff.2023.100546.

[17] M.M. Woldaregay, T.W. Hunde, & V.N. Mishra, *Fitted exact difference method for solutions of a singularly perturbed time delay parabolic PDE*, Partial Differ. Equ. Appl. Math. 8 (2023), 100556. https://doi.org/10.1016/j.padiff.2023.100556.

[18] M. Subhas Abel, J.V. Tawade, & M.M. Nandeppanavar, *MHD flow and heat transfer for the upper-convected Maxwell fluid over a stretching sheet*, Meccanica, 47 (2012), 385-393. https://doi.org/10.1007/s11012-011-9448-7.

[19] S. Mukhopadhyay, *Upper-convected Maxwell fluid flow over an unsteady stretching surface embedded in porous medium subjected to suction/blowing*, Z NATURFORSCH A. 67(10-11) (2012), 641-646. https://doi.org/10.5560/zna.2012-0075.

[20] S. Mukhopadhyay, P. Ranjan De, & G.C. Layek, *Heat transfer characteristics for the Maxwell fluid flow past an unsteady stretching permeable surface embedded in a porous medium with thermal radiation*, J. Appl. Mech. Tech. Phys. 54 (2013), 385-396. https://doi.org/10.1134/S0021894413030061.

[21] S. Nadeem, R.U. Haq, & Z.H. Khan, *Numerical study of MHD boundary layer flow of a Maxwell fluid past a stretching sheet in the presence of nanoparticles*, J Taiwan Inst Chem Eng. 45(1) (2014), 121-126. https://doi.org/10.1016/j.jtice.2013.04.006.

[22] Z. Siri, N.A.C. Ghani, & R.M. Kasmani, *Heat transfer over a steady stretching surface in the presence of suction*, Bound. Value Probl. 2018(1) (2018), 1-16. https://doi.org/10.1186/s13661-018-1019-6.

[23] N.S. Wahid, M.E.H. Hafidzuddin, N.M. Arifin, M. Turkyilmazoglu, & N.A. AbdRahmin, *Magnetohydrodynamic (MHD) Slip Darcy Flow of Viscoelastic Fluid Over A Stretching Sheet and Heat Transfer with Thermal Radiation and Viscous Dissipation*, CFD Lett. 12(1) (2020), 1-12. https://www.akademiabaru.com/submit/index.php/cfdl/article/view/3126.

[24] M. Sankar, Y. Park, J.M. Lopez, & Y. Do, *Double-diffusive convection from a discrete heat and solute source in a vertical porous annulus*, Transp. Porous Media. 91 (2012), 753-775. https://doi.org/10.1007/s11242-011-9871-1.

[25] M. Sankar, J. Park, & Y. Do, *Natural convection in a vertical annuli with discrete heat sources*, Numer. Heat Transf.; A: Appl. 59(8) (2011), 594-615. https://doi.org/10.1080/10407782.2011.561110.

[26] N. Girish, O.D., Makinde, & M. Sankar, *Numerical investigation of developing natural convection in vertical double-passage porous annuli*, Defect Diffus. Forum. 387 (2018), 442-460. Trans Tech Publications Ltd. https://doi.org/10.4028/www.scientific.net/DDF.387.442.

[27] N.K. Reddy, H.K. Swamy, M. Sankar, & B. Jang, *MHD convective flow of Ag–TiO2 hybrid nanofluid in an inclined porous annulus with internal heat generation*, Case Stud. Therm. Eng. 42 (2023), 102719. https://doi.org/10.1016/j.csite.2023.102719.

[28] J.B.J. Fourier, *Theorie analytic da la chaleur*, Paris, 1822 (including papers since 1807, translated 1878). The Analytical Theory of Heat, (2003).

[29] C.I. Christov, *On frame indifferent formulation of the Maxwell–Cattaneo model of finite-speed heat conduction*, Mech. Res. Commun. 36(4) (2009), 481-486. https://doi.org/10.1016/j.mechrescom.2008.11.00316.

[30] V. Tibullo, & V. Zampoli, *A uniqueness result for the Cattaneo–Christov heat conduction model applied to incompressible fluids*, Mech. Res. Commun. 38(1) (2011), 77-79. https://doi.org/10.1016/j.mechrescom.2010.10.008.

[31] M. Ciarletta, & B. Straughan, *Uniqueness and structural stability for the Cattaneo–Christov equations*, Mech. Res. Commun. 37(5) (2010), 445-447. https://doi.org/10.1016/j.mechrescom.2010.06.002.

[32] B. Straughan, *Thermal convection with the Cattaneo–Christov model*, Int. J. Heat Mass Transf. 53(1-3) (2010), 95-98. https:/doi.org/10.1016/j.ijheatmasstransfer.2009.10.001.

[33] S. Han, L. Zheng, C. Li, & X. Zhang, *Coupled flow and heat transfer in viscoelastic fluid with Cattaneo–Christov heat flux model*, Appl. Math. Lett. 38 (2014), 87-93. https://doi.org/10.1016/j.aml.2014.07.013.

[34] M. Mustafa, *Cattaneo - Christov heat flux model for rotating flow and heat transfer of upper-convected Maxwell fluid*, AIP Adv. 5(4) (2015), 047109. https://doi.org/10.1063/1.4917306.

[35] T. Hayat, M. Farooq, A. Alsaedi, & F. Al-Solamy, *Impact of Cattaneo - Christov heat flux in the flow over a stretching sheet with variable thickness*, AIP Adv. 5(8) (2015), 087159. http://dx.doi.org/10.1063/1.4929523.

[36] J. Ahmad Khan, M. Mustafa, T. Hayat, & A. Alsaedi, *Numerical study of Cattaneo - Christov heat flux model for viscoelastic flow due to an exponentially stretching surface*, PLoS One. 10(9) (2015), e0137363. https://doi.org/10.1371/journal.pone.0137363.

[37] F.M. Abbasi, & S.A. Shehzad, *Heat transfer analysis for three-dimensional flow of Maxwell fluid with temperature dependent thermal conductivity: application of Cattaneo - Christov heat flux model*, J. Mol. Liq. 220 (2016), 848-854. https://doi.org/10.1016/j.molliq.2016.04.132.

[38] A. Mushtaq, S. Abbasbandy, M. Mustafa, T. Hayat, & A. Alsaedi, *Numerical solution for Sakiadis flow of upper-convected Maxwell fluid using Cattaneo - Christov heat flux model*, AIP Adv. 6(1) (2016), 015208. https://doi.org/10.1063/1.4940133.

[39] M.I. Khan, M. Waqas, T. Hayat, M.I. Khan, & A. Alsaedi, *Chemically reactive flow of upper-convected Maxwell fluid with Cattaneo–Christov heat flux model*, J. Braz. Soc. Mech. Sci. Eng. 39 (2017), 4571-4578. https://doi.org/10.1007/s40430-017-0915-5.

[40] S.U. Khan, N. Ali, M. Sajid, & T. Hayat, *Heat transfer characteristics in oscillatory hydromagnetic channel flow of Maxwell fluid using Cattaneo Christov model*, Proc. Nat. Acad. Sci. India Sect. A. 89 (2019), 377-385. https://doi.org/10.1007/s40010-017-0470-6.

[41] K.P. Soman, *Insight into wavelets: From theory to practice*, PHI Learning Pvt. Ltd.. (2010).

[42] L. Debnath, & F.A. Shah, *Wavelet transforms and their applications*, (2002), 12-14. Boston: Birkhäuser.

[43] H. Adibi, & P. Assari, *Chebyshev wavelet method for numerical solution of Fredholm integral equations of the first-kind*, Math. Probl. Eng. 2010 (2010). https://doi.org/10.1155/2010/13840817.

[44] S.G. Hosseini, & F. Mohammadi, *A new operational matrix of derivative for Chebyshev wavelets and its applications in solving ordinary differential equations with non analytic solution*, Appl. Math. Sci. 5(51) (2011), 2537-2548. http://www.m-hikari.com/ams/ams-2011/ams-49-52-2011/mohammadiAMS49-52-2011.pdf.

[45] I. Celik, *Numerical solution of differential equations by using Chebyshev wavelet collocation method*, Çankaya Univ. j. sci. eng. 10(2) (2013). https://dergipark.org.tr/en/download/article-file/293746.

[46] I. CELIK, *Chebyshev Wavelet collocation method for solving a class of linear and nonlinear nonlocal boundary value problems*, Fundam. J. Math. Appl. 1(1) (2018), 25-35. https://doi.org/10.33401/fujma.421996.

[47] M.H. Heydari, M.R. Hooshmandasl, & F.M. Ghaini, *A new approach of the Chebyshev wavelets method for partial differential equations with boundary conditions of the telegraph type*, Appl. Math. Model. 38(5-6) (2014), 1597-1606. https://doi.org/10.1016/j.apm.2013.09.013.

[48] U. Saeed, *Wavelet-Galerkin quasilinearization method for nonlinear boundary value problems*, Abstr. Appl. Anal. 2014 (2014, January), Hindawi. https://doi.org/10.1155/2014/868934.

[49] W.M. Abd-Elhameed, E.H. Doha, & Y.H. Youssri, *New spectral second-kind Chebyshev wavelets algorithm for solving linear and nonlinear second-order differential equations involving singular and Bratu type equations*, Abstr. Appl. Anal. 2013 (2013, January), Hindawi. https://doi.org/10.1155/2013/715756.

[50] R.S. Sumana, S. Savitha, & L.N. Achala, *Numerical solution of Fredholm integral equations of second-kind using Haar wavelets*, Comm. Appl. Sci, 4(2) (2016), 49-66. https://www.infinitypress.info/index.php/cas/article/view/1343.

[51] R.S. Sumana, L.N. Achala, & N.M. Bujurke, *Solution of non-homogeneous Burgers' equation by Haar wavelet method*, Int. J. Res. Eng. Sci, 4(6) (2016), 07-16. https://www.ijres.org/papers/Volume%204/v4-i6/Version-3/B4630716.pdf.

[52] R.S. Sumana, L.N. Achala, & N.M. Bujurke, *Numerical solution of non-planar Burgers' equation by Haar wavelet method*, J. Math. Model, 5(2) (2017), 89-118. https://jmm.guilan.ac.ir/article_2460_de6a3c4204cdd70ae58a47355b658fa6.pdf.

[53] K.P. Sumana, L.N. Achala, & V.N. Mishra, *Numerical solution of time-delayed Burgers' equations using Haar wavelets*, Adv. Stud. Contemp. Math. 29(3) (2019), 411-437. http://dx.doi.org/10.17777/ascm2019.29.3.411.

[54] K.P. Sumana, L.N. Achala, & V.N. Mishra, *Numerical simulation of elliptic partial differential equations using 3-scale Haar wavelets*, Adv. Stud. Contemp. Math. 31(3) (2021), 356-376. http://dx.doi.org/10.17777/ascm2021.31.3.355.

[55] M. Usman, T. Zubair, M. Hamid, R.U. Haq, & W. Wang, *Wavelets solution of MHD 3-D fluid flow in the presence of slip and thermal radiation effects*, Phys. Fluids. 30(2) (2018), 023104. https://doi.org/10.1063/1.5016946.

[56] G.E. Awashie, P. Amoako-Yirenkyi, & I.K. Dontwi, *Chebyshev wavelets collocation method for simulating a two-phase flow of immiscible fluids in a reservoir with different capillary effects*, J. Pet. Explor. Prod. Technol. 9(3) (2019), 2039-2051. https://doi.org/10.1007s13202-018-0601-x.

[57] M. Sajid, M.N. Sadiq, K. Mahmood, & N. Ali, *A Legendre wavelet spectral collocation method for analysis of thermal radiation and slip in the oblique stagnation-point flow of Walters-B liquid towards a stretching surface*, Sadhana, 44 (2019), 1-10. https://doi.org/1-10.10.1007/s12046-019-1093-1.

[58] O. Oruc, F. Bulut, & A.L.A.A.T.T.I.N. Esen, *Chebyshev wavelet method for numerical solutions of coupled Burgers' equation*, Hacet. J. Math. Stat. 48(1) (2019), 1-16. https://dergipark.org.tr/en/download/article-file/644612.

[59] S.P. Jakhar, A. Nandal, A. Dhaka, B. Jiang, L. Zhou, & V.N. Mishra, *Fractal feature based image resolution enhancement using wavelet–fractal transformation in gradient domain*, J. Circuits Syst. Comput. 32(02) (2023), 2350035. https://doi.org/10.1142/S0218126623500354.

[60] S.P. Jakhar, A. Nandal, A. Dhaka, B. Jiang, L. Zhou, & V.N. Mishra, *Erratum: Fractal feature based image resolution enhancement using wavelet–fractal transformation in gradient domain*, J. Circuits Syst. Comput. 32(08) (2023), 2392002. https://doi.org/10.1142/S0218126623920020.

[61] R.E. Bellman, & R.E. Kalaba, *Quasilinearization and nonlinear boundary-value problems*, American Elsevier Publishing Co., Inc., New York, (1965).

[62] M.A. Iqbal, U. Khan, A. Ali, & S.T. Mohyud-Din, *Shifted Chebyshev wavelet-quasilinearization technique for MHD squeezing flow between two infinite plates and Jeffery–Hamel flows*, Egypt. j. basic appl. sci. 2(3) (2015), 229-235. https://doi.org/10.1016/j.ejbas2015.05.002.

[63] C.Y. Wang, *Free convection on a vertical stretching surface*, ZAMM Z. fur Angew. Math. Mech. 69(11) (1989), 418-420. https://doi.org/10.1002/zamm.19890691115.

[64] R.S. Reddy Gorla, & I. Sidawi, *Free convection on a vertical stretching surface with suction and blowing*, Appl. Sci. Res. 52 (1994), 247-257. https://link.springer.com/article/10.1007/BF00853952.

[65] W.A. Khan, & I. Pop, *Boundary-layer flow of a nanofluid past a stretching sheet*, Int. J. Heat Mass Transf. 53(11-12) (2010), 2477-2483. https://doi.org/10.1016/j.ijheatmasstransfer.2010.01.032.

[66] R. Malik, M. Khan, A. Shafiq, M. Mushtaq, & M. Hussain, *An analysis of Cattaneo - Christov double diffusion model for Sisko fluid flow with velocity slip*, Results Phys. 7 (2017), 1232- 1237. https://doi.org/10.1016/j.rinp.2017.03.027.

Post Graduate Department of Mathematics and Research Centre in Applied Mathematics, M E S College of Arts, Commerce and Science, 15$^{\text{TH}}$ Cross, Malleshwaram, Bengaluru - 560003, Karnataka, India.
Email address: lakshmibn95@gmail.com

Post Graduate Department of Mathematics and Research Centre in Applied Mathematics, M E S College of Arts, Commerce and Science, 15$^{\text{TH}}$ Cross, Malleshwaram, Bengaluru - 560003, Karnataka, India.
Email address: sumana.shesha@gmail.com

Post Graduate Department of Mathematics and Research Centre in Applied Mathematics, M E S College of Arts, Commerce and Science, 15$^{\text{TH}}$ Cross, Malleshwaram, Bengaluru - 560003, Karnataka, India.
Email address: csasharukmini@gmail.com

Post Graduate Department of Mathematics and Research Centre in Applied Mathematics, M E S College of Arts, Commerce and Science, 15$^{\text{TH}}$ Cross, Malleshwaram, Bengaluru - 560003, Karnataka, India.
Email address: anargund1960@gmail.com

Department of Mathematics, National Institute of Technology, Chaltlang, Aizawl - 796012, Mizoram, India.
Email address: laxmirathour817@gmail.com

Department of Mathematics, School of Advanced Sciences, Vellore Institute of Technology, Vellore - 632014, Tamil Nadu, India.
Email address: lakshminarayanmishra04@gmail.com